[Article] DOI: 10.13208/j.electrochem.2219010 http://electrochem.xmu.edu.cn

Preparation of Highly-Cyclized Sulfurized Polyacrylonitrile for Lithium-Sulfur Batteries

Xuan Ji[1#], Jia-Yu Wang[1#], An-Bang Wang[2], Wei-Kun Wang[2*], Ming Yao[1*], Ya-Qin Huang[1*]

(*1. Beijing Key Laboratory of Electrochemical Process and Technology for Materials, Key Laboratory of Biomedical Materials of Natural Macromolecules, Ministry of Education, Beijing University of Chemical Technology, Beijing 100029, P.R. China; 2. Research Institute of Chemical Defense,Beijing 100191, P.R. China*)

Abstract: Sulfurized polyacrylonitrile (SPAN) is regarded as an attractive cathode candidate of lithium-sulfur (Li-S) batteries for its non-dissolution mechanism and effective alleviation of polysulfides shuttling issue in Li-S batteries, displaying high utilization of cathode active material, outstanding cycle stability and structural stability. However, the relation between cyclization degree and cycle stability of SPAN is still unveiled. In this work, SPAN-C-V composites were synthesized by co-introduction of $CuSO_4$ and zinc *n*-ethyl-*n*-phenyldithiocarbamate (ZDB) in the co-heating of sulfur and polyacrylonitrile. The co-introduction of $CuSO_4$ and ZDB reduced the cyclization reaction onset temperature of PAN while increased the C═C/C=C within SPAN-C-V, thus led to an increase in the degree of cyclization of SPAN-C-V, achieving excellent electrochemical performance by simultaneously improving the cyclization degree and increasing the content of sulfur. The SPAN-C-V exhibited an initial reversible capacity of 805 mAh·g^{-1} and 601 mAh·g^{-1} after 100 cycles with the capacity retention rate of 93% at 0.2 C (1 C = 600 mAh·g^{-1}). The focus on the cyclization degree of SPAN provides an enlightenment of advanced cathode material.

Key words: sulfurized polyacrylonitrile; $CuSO_4$; zinc n-ethyl-n-phenyldithiocarbamate; cyclization degree; lithium-sulfur battery

1 Introduction

As the next-generation of high specific energy secondary batteries, lithium-sulfur (Li-S) batteries have shown high theoretical energy density (2600 Wh·kg^{-1}) and high theoretical capacity (1675 mAh·kg^{-1}). Moreover, elemental sulfur is abundant in nature, low toxicity and low cost of acquiring[1-6]. Consequently, Li-S batteries are rapidly applied in electric vehicles, military and other fields. Nevertheless, there are some drawbacks in the practical application of Li-S batteries. Firstly, the insulating nature of sulfur (5×10^{-30} S·cm^{-1}) hinders electrochemical reactions at a fast rate[7]. Secondly, the discharge products of Li-S batteries are soluble in electrolyte, which block the cathode active material from subsequent reaction and reduce the utilization of sulfur. More severely, the further diffusion to the anode surface will corrode the lithium, causing the bad rechargeable of batteries[8]. Thus, it is of great significance to develop advanced sulfur cathodes with high energy density and long stable cycle life. High-performance conductive polymer-sulfur composites[9], such as polypyrrole, poly-

Cite as: Ji X, Wang J Y, Wang A B, Wang W K, Yao M, Huang Y Q. Preparation of highly-cyclized sulfurized polyacrylonitrile for lithium-sulfur batteries. *J. Electrochem.*, 2022, 28(12): 2219010.

Received: 2022-09-15, Revised: 2022-10-06. #These authors contributed equally to this work and should be considered as co-first authors. *Corresponding author, Wei-Kun Wang, Tel: (86-10)64438266, E-mail: wangweikun2002@163.com Ming Yao, Yaoming@mail.buct.edu.cn, Ya-Qin Huang, Tel: (86-10)64438266, huangyq@mail.buct.edu.cn

acetylene, polyacrylonitrile (PAN), polyaniline and their derivatives, have been a rising research trend[10, 11]. Polymer-sulfur composites can be prepared by co-heating sulfur and conductive polymers, since the co-heating with element sulfur (S) can cause the hydrogen atoms elimination of hydrocarbons and form unsaturated long chains of polymeric pyridine backbone with conjugated electrons[8]. Applying the polymer-sulfur composites as the active material of Li-S batteries can effectively minimize the dissolution of polysulfide, improve the electrochemical performance, and broaden the application of the batteries.

Sulfurized polyacrylonitrile (SPAN) was firstly proposed as a cathode material by Wang et al.[8], obtained by co-heating S and PAN. As the solid-solid conversion mechanism of SPAN, which is distinct from the dissolution and shuttle of polysulfides of traditional Li-S batteries, Li-SPAN batteries show great cycle stability. Additionally, SPAN shows great advantages: (1) high electronic conductivity, (2) suitable for low cost carbonate electrolyte, (3) Coulombic efficiency close to 100%, and (4) low self-discharge rate, which is only 0.8% after 30 days (at 30 ℃)[12].

However, the capacity inferior still hinders the progress of SPAN material, and many outstanding research es of promoting SPAN vulcanization have been achieved. Inspired by the conventional rubber industry, vulcanization accelerators were effectively applied to SPAN to increase the S content and further improve the discharge capacity. Chen et al.[13] employed 2-mercaptobenzothiazoles (MBT) as a vulcanization accelerator, increasing the S content, and improving the discharge capacity and capacity retention significantly. Wang et al.[14] employed diphenyl guanidine (DG) as a vulcanization accelerator which could form polysulfide active group and bond to rubber molecular chain in rubber field. As a result, the S content of SPAN was increased by 12.7wt% and the material exhibited excellent cycling stability. Moreover, the addition of vulcanization accelerator can form larger polysulfide active groups, which can effectively expand the vacancy between PAN chains, provide more vulcanization sites, and increase the S content by forming more C-S bonds and S-S bonds[15]. As for this type of alkaline accelerators, they can reduce the polarity of the active sulfur radical by neutralizing the acidic environment formed by the vulcanization reaction, resulting in a more uniform degree of vulcanization and thus an increase in sulfur loading[16]. In summary, there are many researches that have made great progress in increasing the S content of SPAN, however, the mystery between cyclization degree and electrochemical performance of SPAN is still under veil.

It was speculated that improving the cyclization degree of SPAN could endow SPAN better cycling stability even at high S content. Studies have pointed out that during the co-heating of S and PAN, S will promote the dehydrocyclization of PAN with the increase of temperature, accompanied by hydrogen sulfide (H_2S) production, and then C—S bonds are formed by combining S with polypyridine ring[11]. The cyclization reaction of PAN is similar to the pre-oxidation of PAN fiber. In an early stage of pre-oxidation, PAN fibers undergo intramolecular cyclization and cross-linking, and form an aromatic ring structure under an inert atmosphere[17]. TSE-HAO KO et al.[18] modified PAN fibers with cobalt salts, and cobalt atoms as catalysts could promote the growth and tight buildup of oriented layer planes. Li[19] noticed that PAN fibers treated with copper salts could undergo cyclization reactions at lower temperature. Zhang et al.[20] revealed that the cyclization reaction of PAN was moderated and the onset reaction temperature was reduced by adding nickel salt during the pre-oxidation process of PAN.

Herein, we proposed a co-promotion strategy of cyclization and vulcanization. SPAN-C-V cathode material was successfully synthesized by adding cyclization accelerator copper sulfate ($CuSO_4$) and vulcanization accelerator zinc *n*-ethyl-*n*-phenyldithiocarbamate (ZDB) in the process of co-heating of S and PAN. $CuSO_4$ as cyclization accelerator effectively reduced the cyclization reaction onset temperature of PAN, which can promote the reaction and improve the cyclization degree. ZDB, a common vulcanization

accelerator in traditional rubber industry, can accelerate the cross-linking of unsaturated polyolefin and S, and increase the S content by forming polysulfide active groups. The results showed a relatively high sulfur content of SPAN-C-V (48.01wt%), and a discharge specific capacity of 805 mAh·kg^{-1} for the first cycle at 0.2 C (1 C = 600 mAh·kg^{-1}), and after stably cycled for 100 cycles, the specific capacity maintained at 601 mAh·kg^{-1}.

2 Experimental

2.1 Materials Preparation

The mixture of sulfur (5 g), PAN (1 g), $CuSO_4$ (0.05 g) and ZDB (0.1 g) were ground in an agate mortar for 0.5 h. Then the above mixture was heated in a tube furnace at 400 ℃ for 6 h at a heating rate of 5 ℃·min^{-1}, and the product was heated at 200 ℃ for 30 h at 5 ℃·min^{-1} under an argon atmosphere. The final product is denoted as SPAN-C-V. Decreased the sulfurization reaction temperature to 350 ℃, without the additions of $CuSO_4$ and ZDB in the grinding process, the similar preparation method to that of SPAN-C-V was used, and the product is denoted as SPAN-control. Decreased the sulfurization reaction temperature to 320 ℃, without the addition of $CuSO_4$ in the grinding process, applied the similar preparation method to that of SPAN-C-V, and the obtained product is denoted as SPAN-V.

2.2 Materials Characterization

The morphology and structure of the samples were investigated by scanning electron microscope (SEM, Zeiss Merlin Compact). The elemental contents of the SPAN-control, SPAN-C-V and SPAN-V were measured by organic elemental analysis (CHNS, Elementar Vario EL III). The contents of Cu and Zn in the SPAN-C-V were measured by inductively coupled plasma-optical emission spectrometer (ICP-OES, Aglient 7800). The X-ray diffraction (XRD) patterns of samples were collected using a Rigaku Ultima IV with Cu K_α radiation. X-ray photoelectron spectroscopic (XPS) patterns of samples were recorded using a Thermo Scientific ESCALAB 250Xi with a monochromic Al K_α source (1486.6 eV). *Ex-situ* solid-state nuclear magnetic resonance (SSNMR) of ^{13}C was performed on a Bruker 400M spectrometer. Thermo gravimetric and differential scanning calorimetry (TG-DSC) was measured by PE.

2.3 Electrochemical Measurements

The electrochemical experiments were conducted with CR2025 type coin cells assembled in an argon-filled glove box. The cathodes were prepared by casting the slurry of 70wt% SPAN composites, 20wt% acetylene black and 10wt% LA133 on an Al foil as a current collector. The cathodes were dried in a vacuum oven at 60 ℃ for 24 h and then cut into discs with 14 mm in diameter. The electrolyte was 1 mol·L^{-1} lithium hexafluorophosphate ($LiPF_6$) dissolved in ethylene carbonate/dimethyl carbonate/diethyl carbonate (EC: DMC: DEC, volume ratio = 1: 1:1) with 1% vinylene carbonate (VC) as additive. A Celgard membrane was used as the separator. The diameter and thickness of Li metal anode were 16 mm and 2 mm, respectively. The galvanostatic charge-discharge tests were performed using a LAND BT battery testing system at room temperature within an electrochemical window of 1.0 ~ 3.0 V (vs. Li/Li^+). Electrochemical impedance spectroscopic (EIS) test was carried out on a DR700 workstation in the frequency range from 10^5 to 0.01 Hz with an amplitude of 5 mV. Cyclic voltammetric (CV) curves were measured on CH1608 electrochemical workstation with a scan rate of 0.1 mV·s^{-1} between 1.0 and 3.0 V.

3 Results and Discussion

The SPAN-C-V was prepared by co-introducing $CuSO_4$ and ZDB in the sulfurization process. The XRD data was obtained to ascertain the phase of composites (Figure 1a). The XRD patterns of SPAN-control and SPAN-C-V both show one broad diffraction peak at 25°, which indicates that both SPAN-control and SPAN-C-V still maintained the conjugate structure of π-π stacking with amorphous graphite phase[21, 22]. To explore the chemical composition of SPAN-C-V, XPS was carried out. Figure 1b shows the Cu 2p binding energy spectra of SPAN-C-V composite, and the peaks located at 932.5 eV and 952.5 eV can be assigned to Cu—S bond[23]. The S 2p peak

(Figure 1c) consists of two evident doublets, of which the peaks located at 161.5 eV (S $2p_{3/2}$) and 163.1 eV (S $2p_{1/2}$) can be assigned to C—S bond. And the S $2p_{3/2}$ peak at 163.4 eV is agreement with the C—S bond and Cu—S bond[24], which also verifies the formation of Cu—S bond within the SPAN-C-V. The peak at 164.6 eV (S $2p_{1/2}$) is pertained to S—S bond, demonstrating the existence of short-chain organic sulfide covalently linked to the PAN backbone [24]. The chemical bonding of Cu with S elements in SPAN-C-V was clearly certified by XPS.

The SEM images show that SPAN-C-V was in the shape of spherical nanoparticles with a diameter of about 200 nm, and the corresponding EDS mapping further reveals the uniform distributions of Cu and Zn within the composite (Figure 2). Similar to SPAN-C-V, the SPAN-control was also composed of small spherical particles (Figure 2b), and compared with SPAN-C-V, the particle size of SPAN-control was slightly larger, indicating that the co-introduction of $CuSO_4$ and ZDB did not significantly affect the microscopic morphology of SPAN. The distributions of N, S, Cu and Zn elements in SPAN-C-V were uniform, and the exact elemental contents in the composites were quantified by both elemental analysis and ICP-OES analysis (Table S1). The sulfur contents of SPAN-control, SPAN-V, SPAN-C and SPAN-C-V were 42.82wt%, 54.13wt%, 47.80wt% and 48.01wt%, respectively, representing that not only the vulcanization accelerator can raise the sulfur content, but also the cyclization accelerator and the co-introduction of $CuSO_4$ and ZDB can effectively increase the sulfur content. The Cu and Zn contents in SPAN-C-V were 0.78wt% and 0.79wt%, respectively, confirming the indeed presences of Cu and Zn within the SPAN-C-V.

The ^{13}C SSNMR analyses were performed to reveal

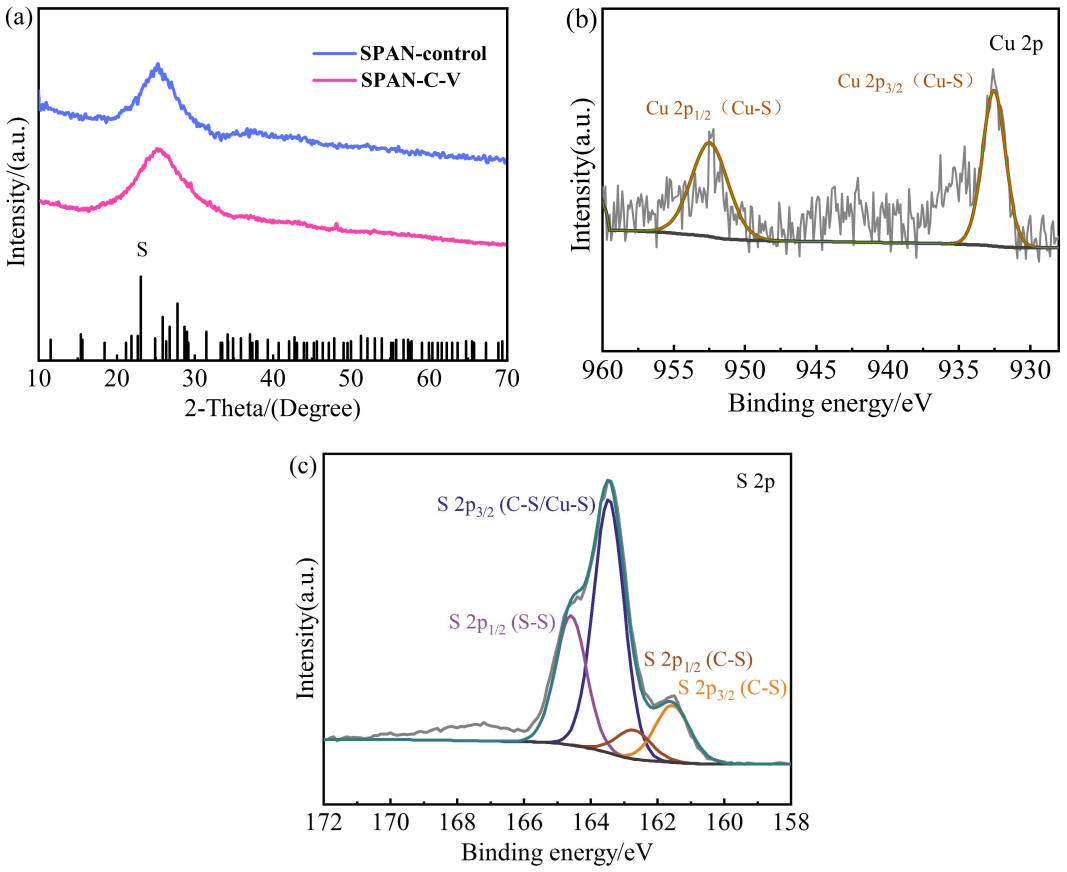

Figure 1 (a) XRD patterns of SPAN-control, SPAN-C-V at 5° · min^{-1} and the standard lines of sublimed sulfur, (b) Cu 2p spectra and (c) S 2p spectra of SPAN-C-V. (color on line)

the structures of PAN, SPAN-control and SPAN-C-V, illustrating the dehydrogenate cyclization reaction processes of SPAN-control and SPAN C-V (Figure 3a). The ^{13}C spectrum of PAN shows two peaks around 121 ppm and 30 ppm, corresponding to the sp hybrid carbon (—CN) of the side-chain and the sp3 hybrid carbon (—CH— and —CH_2—) of the main-chain, respectively[21]. Compared with PAN, the ^{13}C spectra of SPAN-C-V and SPAN-control show two obvious peaks around 150 ppm and 120 ppm, representing the sp^2 hybrid carbon, C=N and C=C, respectively, confirming the promoted cyclization reaction of PAN in the additions of $CuSO_4$ and ZDB[25]. The ^{13}C spectra verify that the —CN group of PAN was cyclized during the heating reaction, i.e., PAN underwent a cyclization reaction during heating[26]. Figure 3b illustrates the DSC curves of several composites. The DSC curves exhibit single exothermic peak which gives the typical cyclization temperature. The cyclization temperatures of PAN-S-C-V and PAN-S-C were lower than that of PAN-S, and the former is higher than the latter, illustrating that cyclization temperature can be effectively lowered by $CuSO_4$ and ZBD together and by $CuSO_4$ alone, and ZDB would react oppositely and increase cyclization temperature.

In order to further confirm the promotion effect of PAN cyclization by $CuSO_4$ and ZDB, C 1s spectra were analyzed (Figure 3c, 3d). The contents of C—C/C=C bond in material were calculated by the product of the peak area ratio of C—C/C=C in C 1s spectrum and the mass ratio of C in the elemental analysis results. The C 1s spectra of SPAN-C-V and SPAN-control were normalized. The calculated peak area ratio of C—C/C=C within SPAN-C-V is 65.4%, while that within SPAN-control is only 55.6%. Combined with the mass ratio of C in the composites from the elemental analysis results (Table S1), the contents of C—C/C=C bond in SPAN-C-V and SPAN-control were calculated to be 23.64wt% and 19.94wt%, respectively. The above results convectively demonstrate that the co-introduction of $CuSO_4$ and ZDB leads to an increase of the C—C/C=C within SPANC-V, resulting in the in creased cyclization structure within SPAN-C-V.

The effect of enhanced cyclization of material on the electrochemical performance of SPAN was further investigated by CV and EIS tests. Figure 4a and Figure 4c show the third CV curves of SPAN-control and SPAN-C-V, respectively. The reduction peak of SPAN-control is at 1.76 V and the oxidation peak is

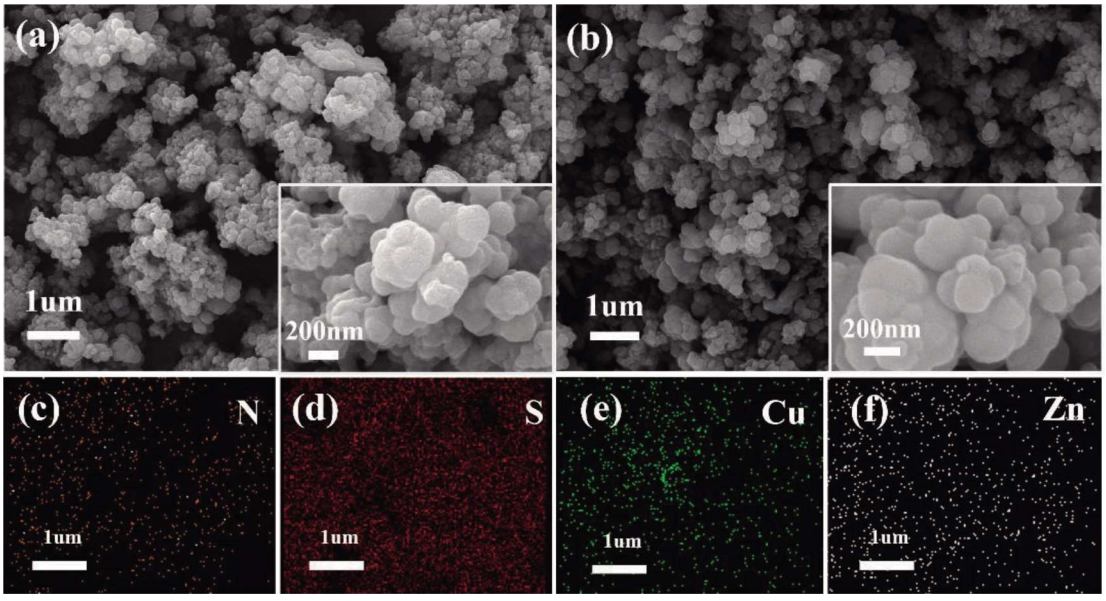

Figure 2 SEM images of (a) SPAN-C-V and (b) SPAN-control, (c-f) EDS elemental mapping images of N, S, Cu and Zn in SPAN-C-V (color on line)

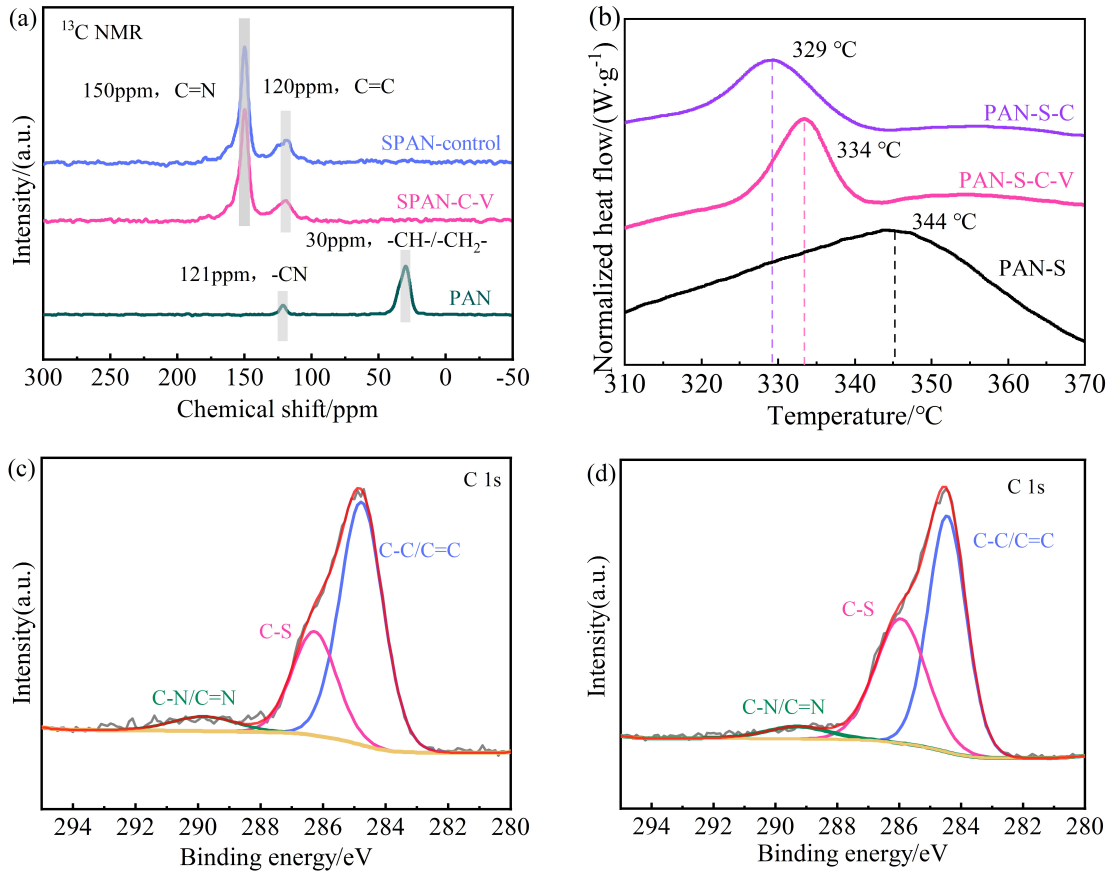

Figure 3 (a) ^{13}C SSNMR spectra of SPAN-control, SPAN-C-V and PAN, (b) DSC curves of the different materials, including mixture of PAN and sulfur (PAN-S), mixture of PAN, sulfur, $CuSO_4$ and ZDB (PAN-S-C-V), and PAN, sulfur and $CuSO_4$ (PAN-S-C), C 1s spectra of (c) SPAN-control and (d) SPAN-C-V. (color on line)

at 2.34 V. As a comparison, the reduction and oxidation peaks of SPAN-C-V are at 1.77 V and 2.32 V respectively. SPAN-control exhibits larger voltage polarization and the lower peak current of SPAN-C-V is also evident from the larger redox peak area and higher current. To further explore the effect of cyclization degree on the reaction kinetics, CV curves of SPAN-control and SPAN-C-V were differentiated (Figure 4b and Figure 4d), showing the onset potentials of oxidation and reduction reactions. According to the common definition in electrochemistry, the current density of 10 $\mu A \cdot cm^{-2}$ beyond the baseline current was counted as the onset potential[27]. The onset potential of the cathodic peak (I) of SPAN-control is 2.41 V, and that of the anodic peak (II) is 1.95 V. Meanwhile, the onset potentials of the cathodic peak and anodic peak of SPAN-C-V are 2.47 V and 1.90 V, respectively. The result represents that the improved cyclization structure leads to an increment in the onset potential of the cathodic peak and a decrement in the onset potential of the anodic peak, thus evidencing the boosting of the redox reaction kinetics. Figure 4e illustrates the EIS spectra of SPAN-control and SPAN-C-V before cycling. Both impedance spectra include a semicircle from high to middle frequency and a slope line in the low frequency. As shown, the charge transfer resistance of SPAN-C-V is much smaller than that of SPAN-control, demonstrating the effective activation and accelerated electrochemical reaction process. After cycling, the charge transfer resistance of SPAN-C-V decreases greatly compared with fresh cells (Figure S4). And SPAN-control shows a new semicircle in high frequency which represents the interface resistance, demon-

strating that solid electrolyte interface (SEI) is formed on the surface of the cathode after charging, hindering the subsequent electrochemical reaction, while SPAN-C-V shows much smaller charge transfer resistance and interface resistance after cycling. The Li^+ diffusion coefficients were further calculated from the EIS plots (Figure 4f). According to the equation (1) [21], the ratio of Li^+ diffu sion coefficient of SPAN-C-V to that of SPAN-control is 25.4, indicating a larger Li^+ diffusion rate.

$$D_{Li^+}=\frac{R^2T^2}{2A^2n^4F^4C^2\sigma^2} \quad (1)$$

On account of the small polarization, and advanced cathodic and anodic onset potentials, the

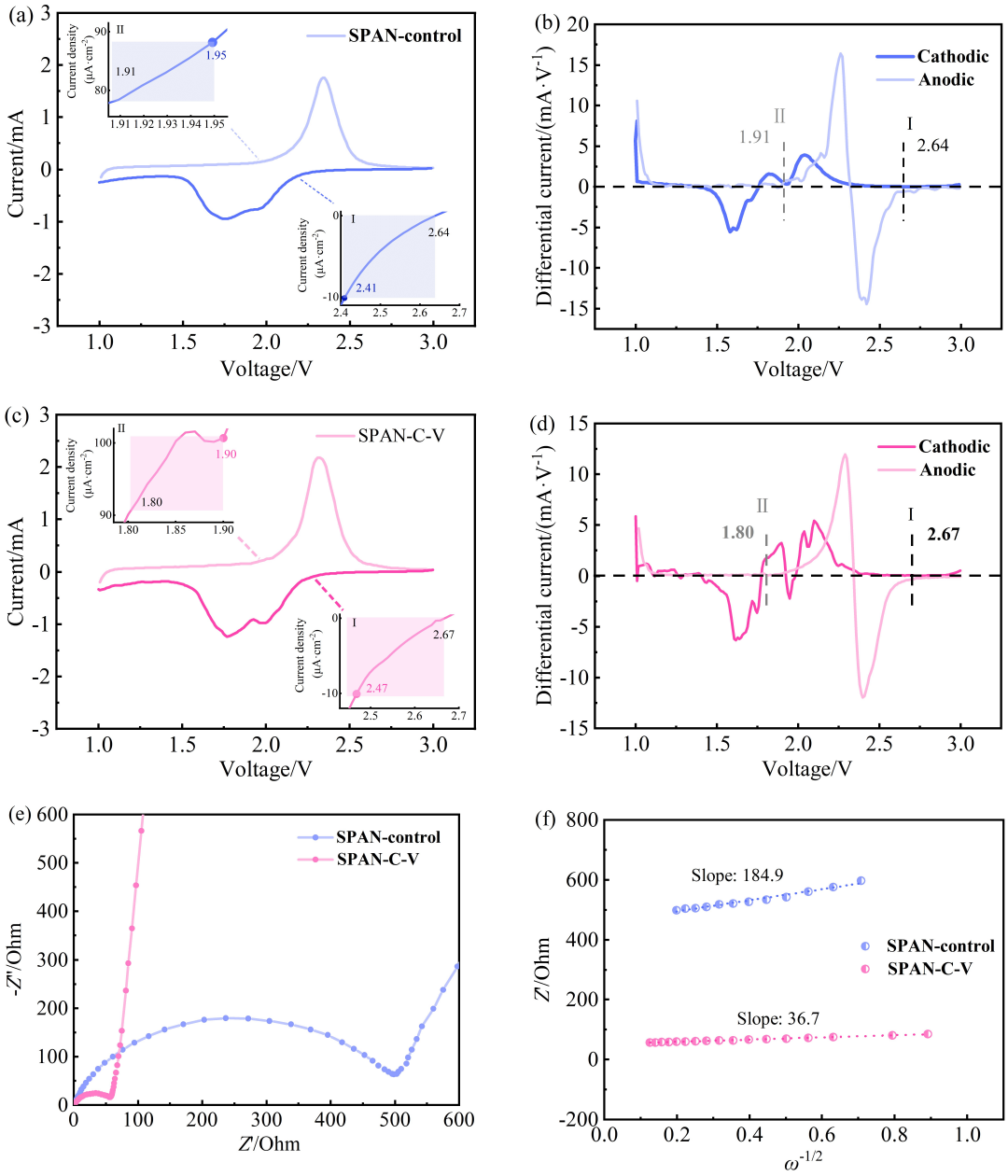

Figure 4 (a) CV curve and corresponding onset potentials of redox peak I and II (inset) of SPAN-control, (b) differential CV curves of SPAN-control, (c) CV curve and corresponding onset potentials of redox peak I and II (inset) of SPAN-C-V, (d) differential CV curves of SPAN-C-V, (e) EIS plots and (f) relationship between Z' and $w^{-1/2}$ in the low-frequency region for SPAN-control and SPAN-C-V. (color on line)

electrochemical performance of SPAN-C-V was evaluated at different rates with area loading of ~1.5 mg·cm^{-2} (SPAN composite as an active material). Figure 5a shows the C-rate capabilities of SPAN-control and SPAN-C-V at a series of current densities. The SPAN-control delivered the reversible discharge capacities of 669, 640, 565, 457 and 288 mAh·kg^{-1}, with the increasing current densities from 0.2, 0.3, 0.5, 1 to 2 C (1 C = 600 mAh·kg^{-1}), respectively, while SPAN-C-V exhibited the enhanced C-rate properties and achieved the reversible discharge capacities of 683, 661, 646, 624 and 571 mAh·kg^{-1}, respectively. In the process of discharging/charging at different C-rates, the discharge capacity of SPAN-C-V varied slightly compared with those of SPAN-control and SPAN-C (Figure S1b). When the C-rate returned to 0.2 C, the discharge capacity of SPAN-C-V reverted to 660 mAh·kg^{-1}, indicating the superior reversibility and better tolerance to the change of current. The charge and discharge curves at different rates of SPAN-C-V exhibited smaller polarization compared with that of SPAN-control, indicating a promoted redox kinetics (Figure 5b, Figure 5c). Figure 5d shows the median voltage difference in the charge and discharge curves of SPAN-control and SPAN-C-V at different C-rates. When discharged at low C-rate (0.2-0.5 C), the electrode structure was relatively stabilized with a small polarization voltage difference, however, at 1 C and 2 C, the voltage difference increased fairly noticeably. The SPAN-C-V maintained a lower polarization voltage all of time, even at high current density of 2 C. Energy efficiency is a pivotal metric for large-scale energy storage systems[27]. The enhanced cyclization degree not only can effectively minimize the voltage hysteresis but also can lead to an increase in energy efficiency (Figure S1a). The

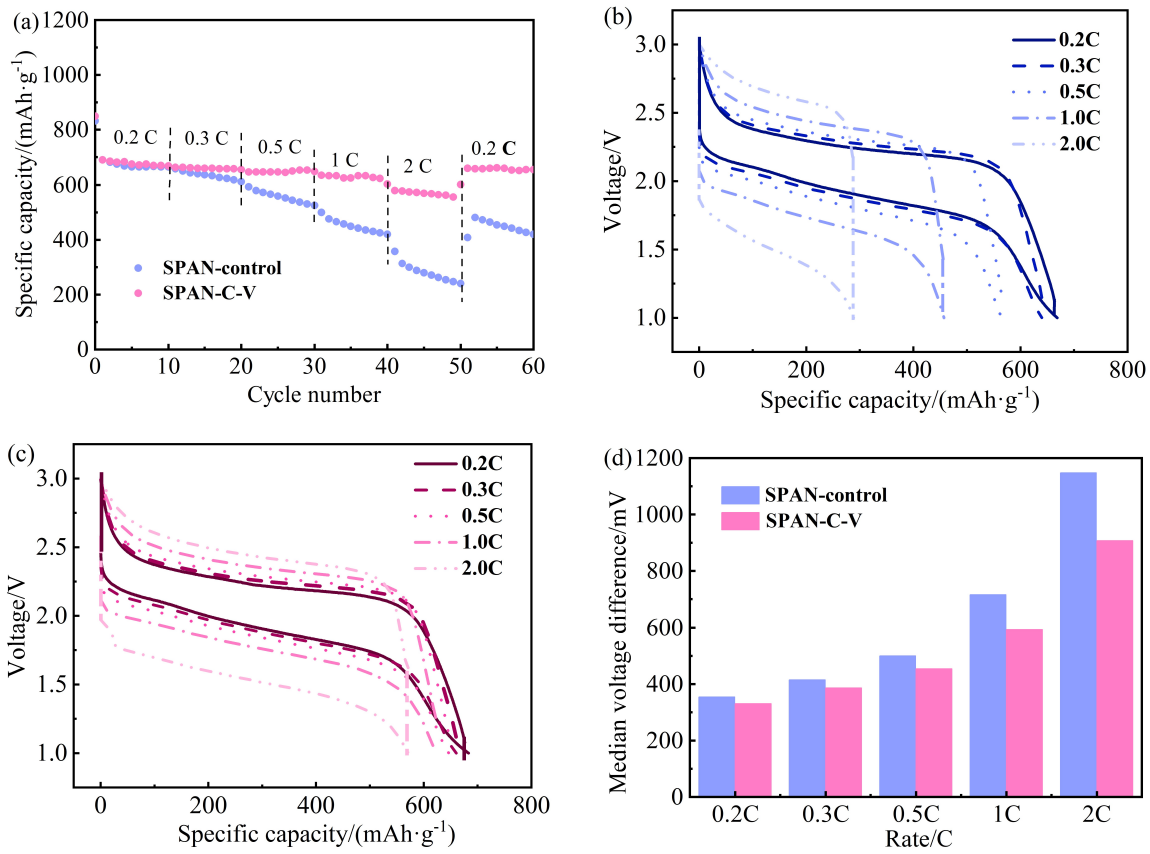

Figure 5 (a) C-rate performances of SPAN-control and SPAN-C-V, (b) Charge and discharge curves of SPAN-control at different C-rates, (c) Charge and discharge curves of SPAN-C-V at different C-rates, (d) Median voltage difference in charge and discharge curves of SPAN-control and SPAN-C-V.

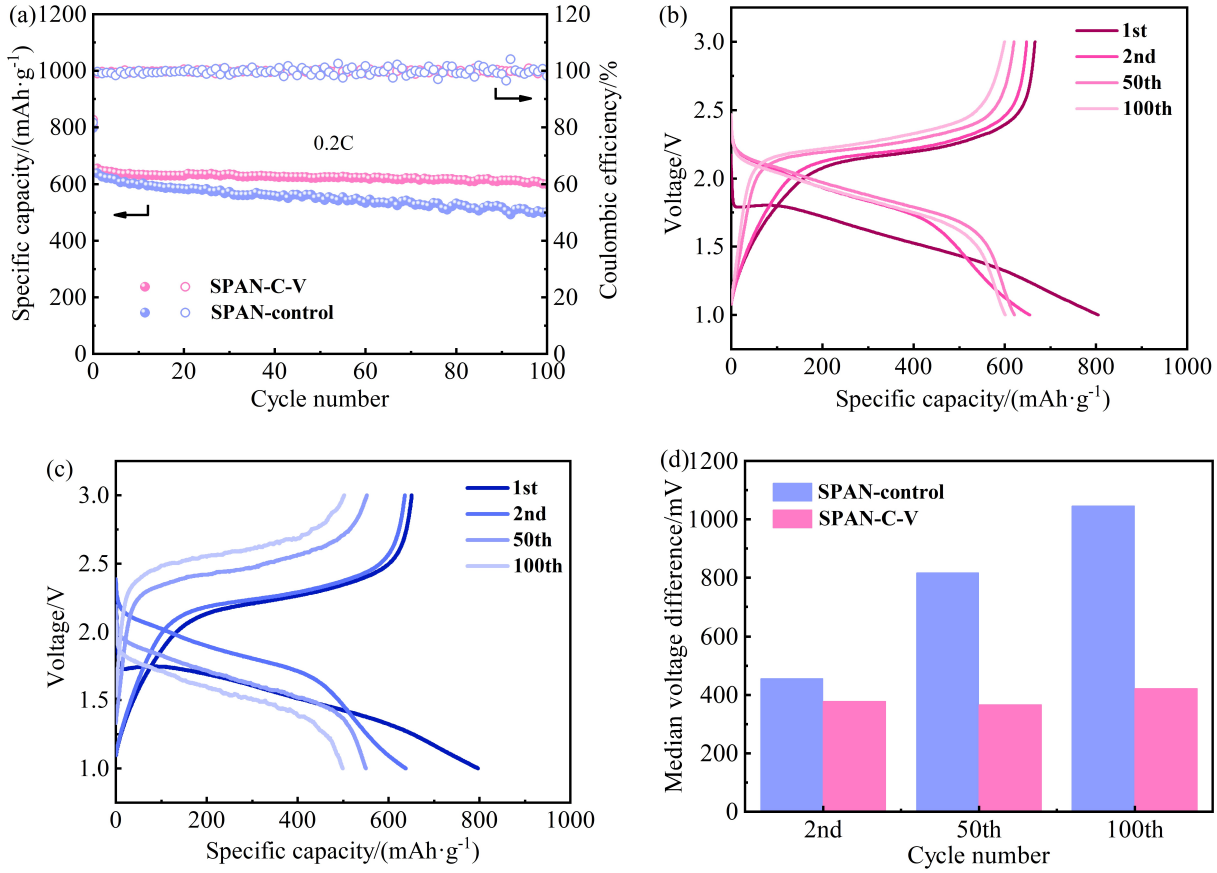

Figure 6 (a) Cycling performances of SPAN-control and SPAN-C-V at 0.2C for 100 cycles, charge and discharge curves at 0.2C of (b) SPAN-C-V and (c) SPAN-control, (d) Median voltage difference plots of charge and discharge curves of SPAN-control and SPAN-C-V. (color on line)

energy efficiency was enhanced from 56% to 63% at 2 C with the co-introduction of $CuSO_4$ and ZDB.

The cycling performances of SPAN-control and SPAN-C-V were tested at 0.2 C (Figure 6a). The SPAN-C-V delivered an initial discharge capacity of 805 mAh·kg^{-1} and 601 mAh·kg^{-1} after 100 cycles. As a comparison, SPAN-control displayed an initial discharge capacity of 797 mAh·kg^{-1} and 499 mAh·kg^{-1} after 100 cycles. Obviously, the capacity of SPAN-control decayed rapidly, while SPAN-C-V exhibited superior capacity retention, and the charge and discharge curves also show the smaller overpotential of SPAN-C-V. To further reveal the effect of cyclization degree on the cycling stability of SPAN, the cycling performance of the SPAN-V at 0.2 C was measured (Figure S2b). The initial discharge capacity of SPAN-V was 829 mAh·kg^{-1} and after 100 cycles the discharge capacity decayed to 287 mAh·kg^{-1}. It is noticeable that the ZDB showed poor performance on the capacity retention of cell, even though it increased the S content of SPAN to a relatively high level (Table S1), which convincingly proves the important role of high cyclization degree in cycling stability. Figure S3 illustrates the capacity retention for SPAN-control and SPAN-C-V at 0.2 C (compared with the 5th cycle, and all the subsequent calculations about capacity retention were based on this criterion). After 100 cycles, the capacity retention rate of SPAN-C-V was 93%, while those of SPAN-control and SPAN-V were 81% and 43% (Figure S2a), respectively, which further demonstrates that the enhanced cyclization degree indeed improves the cycling stability of the SPAN material. In order to show the polarization voltage variation of the cells during the discharge/charge process,

Figure 6d presents the median voltage difference values of charge and discharge curves of SPAN-control and SPAN-C-V, corresponding to the charge and discharge process at 0.2 C. The results indicate that SPAN-C-V consistently displayed a low polarization voltage, signifying a superior redox reversibility of SPAN-C-V. In contrast, the addition of ZDB could only increase the S content by creating active groups with S[14], improve the initial discharge capacity, and reduce the polarization voltage only to a lesser extent (Figure S2d). From the above, it can be confirmed that it is of great importance to improve the cyclization degree of SPAN, and the enhanced cyclization degree leads to smaller transfer resistance, faster Li^+ diffusion and improved redox kinetics, resulting in great cycling stability and rate performance.

4 Conclusions

In this work, the cyclization accelerator $CuSO_4$ and vulcanization accelerator ZDB were employed for the preparation of high-performance SPAN, through which the S content was increased to 48wt%. The structural characterization results of TG-DSC, XPS and organic elemental analysis reveal the improved cyclization degree of SPAN-C-V. As a result, the SPAN-C-V delivered the reversible capacity of 601 $mAh \cdot kg^{-1}$ at 0.2 C with the capacity retention rate of 93% after 100 cycles. Hence, this work provides a positive prospect of high-performance SPAN cathode materials preparation.

References:

[1] Seh Z W, Sun Y, Zhang Q, Cui Y. Designing high-energy lithium-sulfur batteries[J]. Chem. Soc. Rev., 2016, 45(20): 5605-5634.

[2] Manthiram A, Fu Y, Chung S H, Zu C, Su Y S. Rechargeable lithium-sulfur batteries[J]. Chem. Rev., 2014, 114(23): 11751-11787.

[3] Wang L, Zhao J S, He X M, Wan C R. Kinetic investigation of sulfurized polyacrylonitrile cathode material by electrochemical impedance spectroscopy[J]. Electrochim. Acta, 2011, 56(14): 5252-5256.

[4] Ji X, Lee K T, Nazar L F. A highly ordered nanostructured carbon-sulphur cathode for lithium-sulphur batteries[J]. Nat. Mater., 2009, 8(6): 500-506.

[5] Takeuchi T, Kojima T, Kageyama H, Mitsuhara K, Ogawa M, Yamanaka K, Ohta T, Kobayashi H, Nagai R, Ohta A. High capacity sulfurized alcohol composite positive electrode materials applicable for lithium sulfur batteries[J]. J. Electrochem. Soc., 2016, 164(1): A6288-A6293.

[6] He X M, Pu W H, Ren J G, Wang L, Wang J L, Jiang C Y, Wan C R. Charge/discharge characteristics of sulfur composite cathode materials in rechargeable lithium batteries [J]. Electrochim. Acta, 2007, 52(25): 7372-7376.

[7] Yun J H, Kim J H, Kim D K, Lee H W. Suppressing polysulfide dissolution via cohesive forces by interwoven carbon nanofibers for high-areal-capacity lithium-sulfur batteries[J]. Nano Lett., 2017, 18(1): 475-481.

[8] Wang J L, Yang J, Wan C R, Du K, Xie J Y, Xu N X. Sulfur composite cathode materials for rechargeable lithium batteries[J]. Adv. Funct. Mater., 2003, 13(6): 487-492.

[9] Zhang T, Hong M, Yang J, Xu Z X, Wang J L, Guo Y S, Liang C D. A high performance lithium-ion-sulfur battery with a free-standing carbon matrix supported Li-rich alloy anode[J]. Chem. Sci., 2018, 9(47): 8829-8835.

[10] Yang H J, Chen J H, Yang J, Wang J L. Prospect of sulfurized pyrolyzed poly(acrylonitrile) (S@pPAN) cathode materials for rechargeable lithium batteries[J]. Angew. Chem. Int. Edit., 2020, 59(19): 7306-7318.

[11] Ahmed M S, Lee S, Agostini M, Jeong M G, Jung H G, Ming J, Sun Y K, Kim J, Hwang J Y. Multiscale understanding of covalently fixed sulfur-polyacrylonitrile composite as advanced cathode for metal-sulfur batteries[J]. Adv. Sci., 2021, 8(21): e2101123.

[12] Wang L, He X M, Li J J, Gao J, Fang M, Tian G Y, Wang J L, Fan S S. Graphene-coated plastic film as current collector for lithium/sulfur batteries[J]. J. Power Sources, 2013, 239: 623-627.

[13] Chen H W, Wang C H, Hu C J, Zhang J S, Gao S, Lu W, Chen L W. Vulcanization accelerator enabled sulfurized carbon material for high capacity high stability lithium-sulfur batteries[J]. J. Mater. Chem. A, 2015, 3: 1392.

[14] Wang Y, Shuai Y, Chen K H. Diphenyl guanidine as vulcanization accelerators in sulfurized polyacrylonitrile for high performance lithium-sulfur battery[J]. Chem. Eng. J., 2020, 388: 124378.

[15] Wang Y, Zhang Y P, Shuai Y, Chen K H. Diphenyl guanidine vulcanization accelerators enable sulfurized polyacrylonitrile cathode for high capacity and ether-compatible by fast kinetic[J]. Energy, 2021, 233: 121160.

[16] Jin J, van Swaaij A P J, Noordermeer J W M, Blume A, Dierkes W K. On the various roles of 1,3-DIPHENYL Guanidine in silica/silane reinforced sbr/br blends[J]. Polym. Test., 2021, 93: 106858.

[17] Liu R G, Xu J. Recent progress in high performance PAN based carbon fibers[J]. Sci. Tech. review, 2018, 36(19): 32-42.

[18] KO T H, Huang L C. Preparation of high-performance carbon fibres from PAN fibres modified with cobaltous chloride[J]. J. Mater. Sci., 1992, 27(9): 2429-2436.

[19] Li J M. The effect of cuprous salt on polyacrylonitrile fiber(PAN) during thermostablization[J]. J. China Textile University, 1992, 18(4): 22-29.

[20] Zhang W X, Wang Y Z, Wang Y X, Cai H S, Li M S. Effect of $NiSO_4$ on the structure and properties of PAN precursors and resultant carbon fibres[J]. Acta Polym. Sin., 2001, (5): 670-673.

[21] Ma S B, Zhang Z G, Wang Y, Yu Z J, Cui C, He M X, Huo H, Yin G P, Zuo P J. Iodine-doped sulfurized polyacrylonitrile with enhanced electrochemical performance for lithium sulfur batteries in carbonate electrolyte. [J]. Chem. Eng. J., 2021, 418: 129410.

[22] Wang J, He Y S, Yang J. Sulfur-based composite cathode materials for high-energy rechargeable lithium batteries [J]. Adv. Mater., 2015, 27(3): 569-575.

[23] Dou T, Qin Y, Zhang F Z, Lei X D. CuS nanosheet arrays for electrochemical CO_2 reduction with surface reconstruction and the effect on selective formation of formate [J]. ACS Appl. Energy Mater., 2021, 4(5): 4376-4384.

[24] Jin Z Q, Liu Y G, Wang W K, Wang A B, Hu B W, Shen M, Gao T, Zhao P C, Yang Y S. A new insight into the lithium storage mechanism of sulfurized polyacrylonitrile with no soluble intermediates[J]. Energy Storage Mater., 2018, 14: 272-278.

[25] Ratanavaraporn J, Soontornvipart K, Shuangshoti S, Shuangshoti S, Damrongsakkul S. Localized delivery of curcumin from injectable gelatin/Thai silk fibroin microspheres for anti-inflammatory treatment of osteoarthritis in a rat model[J]. Inflammopharmacology, 2017, 25(2): 211-221.

[26] Wang Y S, Xu L H, Wang M Z, Pang W M, Ge X W. Structural identification of polyacrylonitrile during thermal treatment by selective ^{13}C labeling and solid-state ^{13}C NMR spectroscopy[J]. Macromolecules, 2014, 47(12): 3901-3908.

[27] Yuan Z, Peng H J, Hou T Z, Huang J Q, Chen C M, Wang D W, Cheng X B, Wei F, Zhang Q. Powering lithium-sulfur battery performance by propelling polysulfide redox at sulfiphilic hosts[J]. Nano Lett., 2016, 16(1): 519-527.

锂硫电池用高度环化硫化聚丙烯腈的制备

姬 璇[1#],汪佳裕[1#],王安邦[2],王维坤[2*],姚 明[1*],黄雅钦[1*]

(1. 材料电化学过程与技术北京市重点实验室,天然高分子生物医用材料教育部重点实验室,
北京化工大学,北京 100029; 2. 防化研究院,北京 100191)

摘要: 硫化聚丙烯腈因其不溶解机制和有效缓解锂硫电池中多硫化物“穿梭效应”,被认为是具有吸引力的锂硫电池正极候选材料。硫化聚丙烯腈的导电聚合物骨架具有优异的电子导电性,同时共轭主链能有效解决充放电过程中硫正极体积变化引起的正极结构坍塌问题。因硫化聚丙烯腈的固-固反应机理,有效克服了传统硫正极在醚类电解液中多硫化物溶解及穿梭效应的问题,具有高正极活性物质利用率、出色的循环稳定性和结构稳定性等优势。有许多研究工作致力于通过硫化促进剂来提高硫化聚丙烯腈的硫含量,进而提高材料的能量密度。其中,硫化聚丙烯腈主链的环化度与循环稳定性的关系引起了我们的关注。在该研究工作中,通过在硫化过程中引入无水硫酸铜和正乙基正苯基二硫代氨基甲酸锌(ZDB)合成了SPAN-C-V 复合材料。无水硫酸铜和 ZDB 的共同引入降低了聚丙烯腈环化反应的起始温度,同时提高了产物 SPAN-C-V 内碳碳双键的含量,在提高了材料硫含量的同时提高了其环化度。以 SPAN-C-V 为正极活性物质所组装的锂硫电池展现出良好的循环稳定性和倍率性能:在 0.2 C (1 C = 600 mAh·kg^{-1})下循环 100 次后的可逆容量为 601 mAh·kg^{-1},容量保持率为93%。该工作对于硫化聚丙烯腈材料的发展提供了参考。

关键字: 硫化聚丙烯腈;$CuSO_4$;正乙基正苯基二硫代氨基甲酸锌;环化度;锂硫电池